Chiara Ricca and **Ulrich Aschauer**

View Online   Export Citation   CrossMark

Photochemical anisotropy and direction-dependent optical absorption in semiconductors

View Online   Export Citation   CrossMark

Chiara Ricca[1,2] and Ulrich Aschauer[1,2,a] (iD)

AFFILIATIONS

[1] Department of Chemistry and Biochemistry, University of Bern, Freiestrasse 3, CH-3012 Bern, Switzerland

[2] National Centre for Computational Design and Discovery of Novel Materials (MARVEL), CH-3012 Bern, Switzerland

[a] Author to whom correspondence should be addressed: ulrich.aschauer@unibe.ch

ABSTRACT

Photochemical reactions on semiconductors are anisotropic, since they occur with different rates on surfaces of different orientations. Understanding the origin of this anisotropy is crucial to engineering more efficient photocatalysts. In this work, we use hybrid density functional theory to identify the surfaces associated with the largest number of photo-generated carriers in different semiconductors. For each material, we create a spherical heat map of the probability of optical transitions at different wave vectors. These maps allow us to identify the directions associated with the majority of the photo-generated carriers and can, thus, be used to make predictions about the most reactive surfaces for photochemical applications. The results indicate that it is generally possible to correlate the heat maps with the anisotropy of the bands observed in conventional band structure plots, as previously suggested. However, we also demonstrate that conventional band structure plots do not always provide all the information and that taking into account the contribution of all possible transitions weighted by their transition dipole moments is crucial to obtain a complete picture.

I. INTRODUCTION

Since Fujishima and Honda, for the first time, reported H_2 production from water using TiO_2-based photoelectrodes in 1972,[1] semiconductor-based heterogeneous photocatalysis has received great attention due to the increasing energy demand and diminishing fossil resources. Indeed, heterogeneous photocatalytic processes, such as photocatalytic water splitting (water oxidation and hydrogen reduction), artificial photosynthesis (CO_2 reduction), or the degradation of pollutants, constitute one of the most promising solutions for environmental and energy sustainability via direct harvesting of solar energy.[2–5]

It is well accepted that photocatalytic reactions involve three sequential processes. First, electron/hole pairs are photo-generated when the semiconductor is illuminated by light with an energy equal to or greater than the material's bandgap, which leads to excitation of electrons from the valence (VB) to the conduction band (CB). While recombination of electron/hole pairs can occur in the bulk, a fraction of the generated electrons and holes migrate, in

a second step, toward the surfaces of the catalyst, where they can initiate reduction and oxidation reactions in a final step, respectively. However, these reactions can be driven by the photo-generated electrons and holes only if the reduction and oxidation potentials of the targeted reaction lie within the CB and VB of the material, respectively. According to the relative position of the VB and CB and the redox potential of specific reactions, it is possible to identify different types of catalysts: (i) strongly oxidative semiconductors with sufficiently positive VB potentials to produce OH radicals, such as SnO_2, $BiVO_4$, TiO_2, and WO_3 (see the left side of Fig. 1), which are promising candidates for the photo-degradation of organic pollutants; (ii) strongly reductive catalysts with the CB position more negative than the hydrogen evolution and CO_2 reduction potentials, such as Cu_2O, Bi_2Se_3, SiC, and Si (see the right side of Fig. 1), which are promising semiconductors for solar-fuel production under visible light; and (iii) materials with VB/CB potential more positive/negative than the H_2/O_2 evolution potentials that are suitable to catalyze the overall water splitting reaction (see the pink shaded area in Fig. 1).[3]
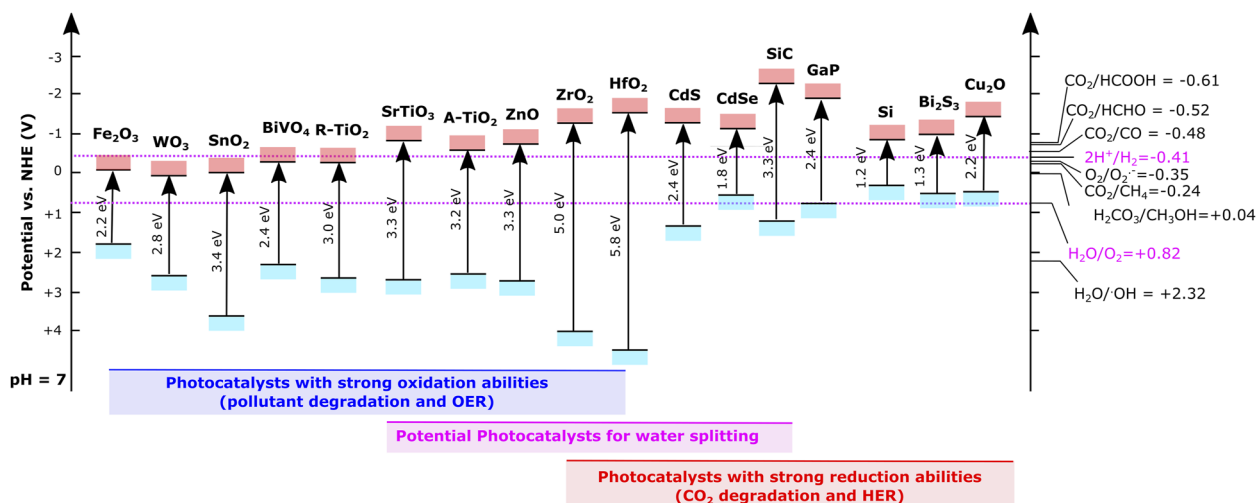
FIG. 1. Band-edge positions of some typical semiconductor photocatalysts relative to the energy levels of the redox couples involved several photocatalytic processes. Adapted from Ref. 3.

Hundreds of materials are currently available for different photocatalytic applications; however, so far, no semiconductor is able to meet all the requirements in terms of efficiency, stability, safety, cost, and ability to absorb solar energy. Efforts to design new materials or to improve the performance of already existing ones can benefit from a deeper understanding of the fundamental properties and mechanisms leading to the observed behavior. For example, it is well known that photochemical reactions on semiconductors are anisotropic, since they occur with different rates on surfaces of different orientations that, hence, have different photocatalytic activities toward reduction and oxidation reactions.[6–10] Despite this phenomenon being fundamental for the design of photocatalysts, the underlying mechanism is not well understood.[10] Giocondi *et al.*[10] suggested, as a general principle, that the observed anisotropic photochemical reactivity can be explained by the spectral distribution of the incident light and the anisotropic dispersion of the photocatalyst's electronic band structure: the lowest energy photons that are able to initiate optical transitions will lead to charge carriers with wave vectors aligned with the transition's position in reciprocal space. The photo-generated carriers will, therefore, preferentially migrate to surfaces perpendicular to that wave vector, leading to an increased reactivity of these surfaces. Using this concept, they explained the observed larger activity of the (100) surface of SrTiO₃ micro-crystals compared to the (110) and (111) surfaces toward both oxidation and reduction reactions. Photons with energies larger than the bandgap (3.25 eV) and up to 4.1 eV (maximum within the experimental setup) can excite transitions near the Γ-point, some along the [110] and [111] directions, but the large majority along the [100] direction, where the bands are weakly dispersive (flat). The electronic band structure of the material, thus, favors the creation of photo-generated carriers with wave vector perpendicular to the (100) surface. The authors suggest that this is a fundamental principle applicable not only to SrTiO₃, but also to all photocatalysts. We note here that, as explained in Ref. 10, there can be several reasons for the surface perpendicular

to which most carriers are created to not appear as most reactive in experiments: phonon scattering resulting in a change of the carrier momentum and recombination of the carriers in the bulk or at surface or defect states that act as traps are only some of the possible explanations. Nevertheless, the principle reflects a fundamental property of photocatalysts and can be invoked to predict the photochemical anisotropy of semiconductor materials.

Density functional theory (DFT) is a valuable tool for material design and discovery. In particular, hybrid DFT can provide accurate structural and electronic properties of semiconductors.[11–13] It can also be used to predict optical properties of materials.[14–16] Quantities such as the absorption coefficient can be derived from the frequency-dependent dielectric function, computed within the independent particle approximation. This consists of an imaginary part determined as a summation over CB states, and a real part, obtained from the Kramers–Kronig transformation.[14] According to Fermi's golden rule, the optical absorption of a semiconductor at a photon energy $\hbar\omega$ is proportional to[17]

$$\frac{2\pi}{\hbar} \frac{1}{4\pi^3} \int \left| \langle v_{\vec{k}} | \vec{p} | c_{\vec{k}} \rangle \right|^2 \delta(E_{c,\vec{k}} - E_{v,\vec{k}} - \hbar\omega) d\vec{k}, \quad (1)$$

where the Brillouin-zone integral sums the joint density of states at energy $\hbar\omega$ over different $\vec{k}$ vectors and $\langle v_{\vec{k}} | \vec{p} | c_{\vec{k}} \rangle$ is the transition dipole moment (TDM) matrix, i.e., the electric dipole moment associated with a transition from a valence state $v_{\vec{k}}$ to a conduction state $c_{\vec{k}}$. The direction of TDM gives the polarization of the transition and determines how the system will interact with an electromagnetic wave of a given polarization, while the square of its norm represents the probability for a transition between the two states to occur.

In this work, we use hybrid DFT to investigate the anisotropy of the optical absorption of different photocatalysts by creating spherical heat maps of optical-transition probabilities along different directions in space, when the material interacts with photons within a specific energy range. These direction-dependent maps

of the optical absorption identify wave vectors associated with the majority of photo-generated carriers upon irradiation with light of a specific energy. Hence, they can be used to make predictions about the most reactive surfaces for photochemical applications, as suggested in Ref. 10. However, different from Ref. 10, our predictions do not only reflect the dispersion of the material's electronic band structure as shown in conventional two-dimensional (2D) band structure plots, but they take into account the full three-dimensional (3D) band structure as well as the probability for each transition to occur (transition allowed or forbidden by the selection rules) via the calculation of the TDM. Indeed, while in the majority of cases, results can be explained by a straightforward comparison of the heat map with the 2D electronic band structure together with the hypothesis suggested by Giocondi *et al.*; more generally, taking into account all possible transitions weighted by the corresponding transition dipole moments is crucial to obtain a complete picture.

II. METHODS

DFT calculations were carried out with the Vienna *Ab initio* Simulation Package (VASP)[18–21] using the Heyd–Scuseria–Ernzerhof (HSE)[22,23] hybrid exchange–correlation functional. Projector augmented-wave potentials[24,25] were used with a plane-wave cut-off of 500 eV. Space group, magnetic properties, and dimension of the Γ-centered k-mesh used to sample the Brillouin zone, as well as the type of pseudopotential and the percentage of exact exchange used to model the primitive cell of various materials, are reported in Table S1 of the supplementary material. All internal and lattice parameters were relaxed with a force threshold of 10^{-3} eV/Å. This setup provides excellent agreement with experiment (see the supplementary material, Sec. S2). Optical properties of the materials were obtained via the calculation of the frequency-dependent dielectric function within the independent particle approximation[14] and analyzed using the pymatgen Wavederf module.[26]

The direction-dependent probability of a material to absorb photons in a given wavelength range (λ_{min} to λ_{max}) was mapped on spherical heat maps obtained by projecting the k-mesh used to sample the reciprocal space on the surface of a unit sphere centered at the origin of the reciprocal lattice. Each k-point is associated with an absorption coefficient (P_k) computed by summing over the square of the TDM for transitions between bands $v_{\vec{k}}$ and $c_{\vec{k}}$ at that k-point $\vec{k}$, if the wavelength (λ_{vc}) of the transition is within the considered energy range (λ_{min} to λ_{max}),

$$P_{\vec{k}} = \sum_{vc}^{\lambda_{min} < \lambda_{vc} < \lambda_{max}} |\langle v_{\vec{k}} | \vec{p} | c_{\vec{k}} \rangle|^2. \tag{2}$$

The final spherical heat map of direction-dependent absorption is created by interpolating the obtained discrete data onto a regular grid in spherical coordinates, which we represent in a cylindrical projection as schematized in Fig. 2. We considered transitions in the energy range going from the bandgap (E_g) of each material up to a minimum energy ($E_g + \Delta E$) necessary to observe vertical transitions (cf. Table S1).
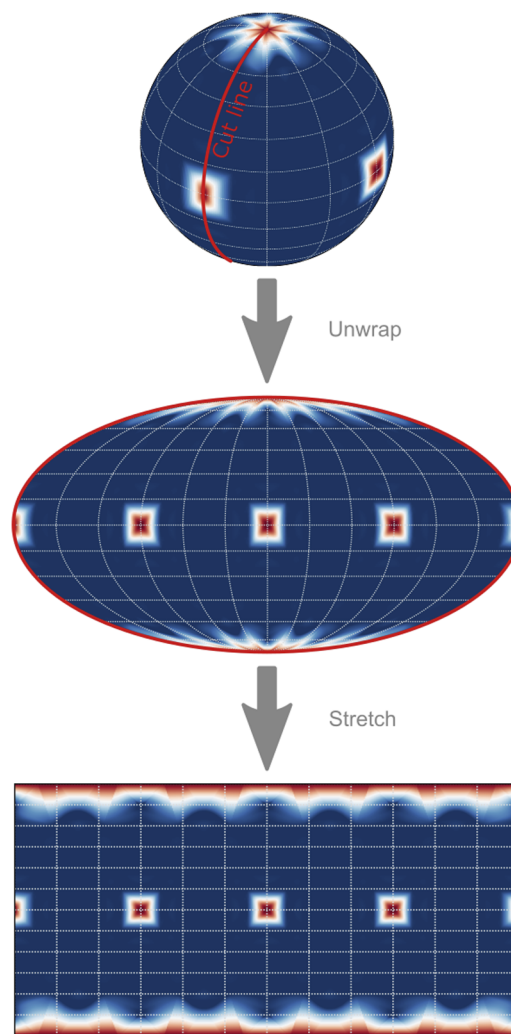

FIG. 2. Schematic of the process of passing from the spherical heat map to the final cylindrical projection.

III. RESULTS AND DISCUSSION

Giocondi *et al.*[10] investigated the anisotropic reactivity of $SrTiO_3$ using photochemical reactions that deposit insoluble products on the surface of $SrTiO_3$ micro-crystals. Their results indicated that {100} surfaces are most reactive. This observation was explained considering that the majority of electron–hole pairs used for photochemical reactions is created by photons with energies greater than the bandgap but lower than 4.1 eV and that, according to the band structure of $SrTiO_3$, photons with these energies can excite a larger number of transitions along [100] than other directions due to the weakly dispersive bands along this direction.

The heat map of Fig. 3(a) shows the direction-dependent probability of $SrTiO_3$ to absorb photons with energies up to 4.1 eV, computed according to the procedure described in Sec. II. In agreement with the experimental observations, we predict the {100} surfaces to be most active for photochemical processes, since the largest
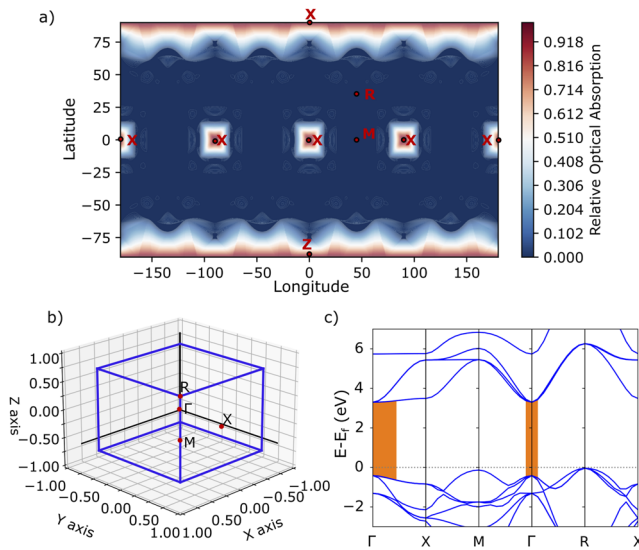
FIG. 3. (a) Heat map of the direction-dependent optical absorption shown as a cylindrical projection along with the position and labels of the high symmetry points, (b) Brillouin zone, and (c) band structure plot for SrTiO$_3$. The shaded regions indicate momentum states, where vertical transitions are possible, when the photon energy is equal to E_g(SrTiO$_3$) + 0.8 eV.

TABLE I. Directions associated with the largest number of photo-generated carriers according to the conventional 2D-band structure or our 3D-direction-dependent optical absorption plots.

Material	Space group	2D-band structure	3D-plots
ZrO$_2$	$P2_1/c$	C-[$\bar{1}01$]	C$'$-[$\bar{1}0\bar{1}$]
HfO$_2$	$P2_1/c$	X-[$\bar{1}00$]	X-[$\bar{1}00$]
WO$_3$	$P2_1/c$	B-[001]	B-[001]
TiO$_2$-A	$I4_1/amd$	Z-[001]	Z-[001]
TiO$_2$-R	$P4_2/mnm$	X-[010]	Z-[001]
WO$_3$	$P4_2/mnm$	Z-[001]	Z-[001]
SnO$_2$	$P4_2/mnm$	X-[010]	X-[010]
Fe$_2$O$_3$	$R\bar{3}c$	F-[110]	Z-[111]
		L-[100]	
Bi$_2$Se$_3$	$R\bar{3}m$	Z-[111]	Z-[111]
ZnO	$P6_3mc$	A-[001]	A-[001]
		M-[100]	M-[100]
SiC	$P6_3mc$	M-[100]	M-[100]
CdSe	$P6_3mc$	A-[001]	A-[001]
		M-[100]	M-[100]
CdS	$P6_3mc$	A-[001]	A-[001]
		M-[100]	M-[100]
Bi$_2$S$_3$	$Pnma$	Z-[001]	Z-[001]
		T-[011]	T-[011]
		Y-[010]	Y-[010]
		X-[100]	
CH$_3$NH$_3$PbI$_3$	$Pnma$	Z-[001]	Z-[001]
SiC	$F\bar{4}3m$	X-[101]	X-[101]
GaP	$F\bar{4}3m$	L-[111]	L-[111]
CdSe	$F\bar{4}3m$	L-[111]	L-[111]
CdS	$F\bar{4}3m$	L-[111]	L-[111]
SrTiO$_3$	$Pm\bar{3}m$	X-[100]	X-[100]
Cu$_2$O	$Pm\bar{3}m$	X-[100]	X-[100]
CsPbI$_3$	$Pm\bar{3}m$	R-[111]	R-[111]
Si	$Fd\bar{3}m$	L-[111]	L-[111]

absorption is observed projected on this direction. As suggested in Ref. 10, this result can be rationalized using arguments based on the computed band structure: photons with energies between the SrTiO$_3$ bandgap and 4.1 eV can excite transitions near the Γ-point, with excited states in the [100] [Γ to X, cf. Figs. 3(b) and S2 in the supplementary material], [110] (Γ to M), or [111] (Γ to R) directions as shown by the shaded regions in Fig. 3(c). However, the flat character of the bands in the Γ to X direction results in a much larger number of photo-generated carriers with wave-vector perpendicular to the (100) surface, explaining the larger absorption intensity along this direction (see Table I for a comparison of the direction associated with the largest number of photo-generated carriers according to the band structure and our optical-absorption plots).

When the same procedure is applied to other photocatalyst materials, the argument based on the conventional 2D band structure plots is verified in the majority of cases. For example, our heat map for GaP in Fig. 4(a) confirms the suggestion by Giocondi et al.[10] that for materials with the zinc-blende structure the most reactive orientation should be (111). Indeed, photons with energies between the GaP bandgap and 4.0 eV can excite transitions near the Γ-point with excited states in the [111] direction [Γ to L, cf. Figs. 4(c) and S2 in the supplementary material].

However, there are materials for which the conventional 2D band structure does not seem to provide all the necessary information to correctly predict the most reactive surface orientation. For example, the band structure computed for the rutile polymorph of TiO$_2$ in Fig. 5(c) suggests that the largest number of excited transitions induced by photons of energy larger than the bandgap (E_g) up to E_g + 0.8 eV takes place from Γ to X ([100] direction) and from Γ to M ([110] direction) and with a smaller contribution also

from Γ to Z ([001] direction). Do due the less dispersive character of the 2D bands along the first two directions, one would expect the (110) and (100) surfaces to be more reactive than the (001) surface. The heat map of the direction-dependent optical absorption of Fig. 5(a) suggests, instead, that photo-generated carriers with wave-vectors perpendicular to this latter surface should be most abundant, followed by carriers with wave-vectors perpendicular to [110]. In order to explain this apparent contradiction, we computed the TDM for a vertical transition from the top of the valence band to the bottom of the conduction band at the k-points Z (12.3 D^2), M (2.0 D^2), and X (0.2 D^2) using the VASPKIT package.[27] Based on these TDM values, we conclude that, even though the flattest path in the band structure is from Γ to M or Γ to X, the larger probability for transitions at the Z point leads to photo-generated carriers with wave-vectors perpendicular to [001] to be most abundant.

These results could help understand the experimental results for rutile that are often contradictory and obtained under different experimental conditions, for different photochemical reactions, and on different types of samples. For example, Ohno et al.[8] reported
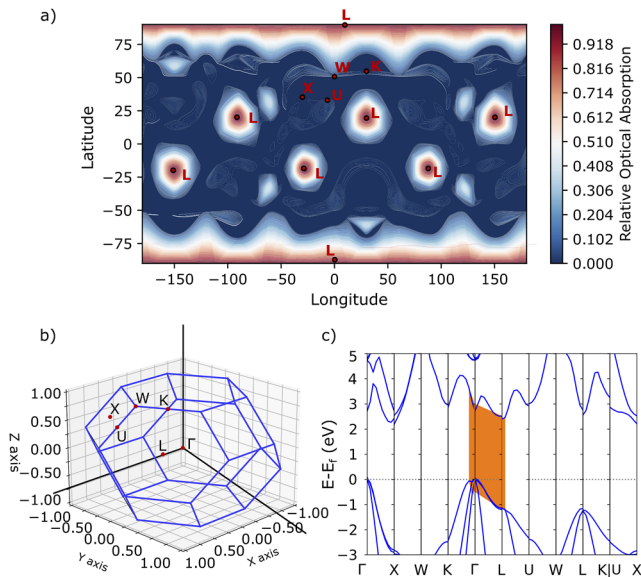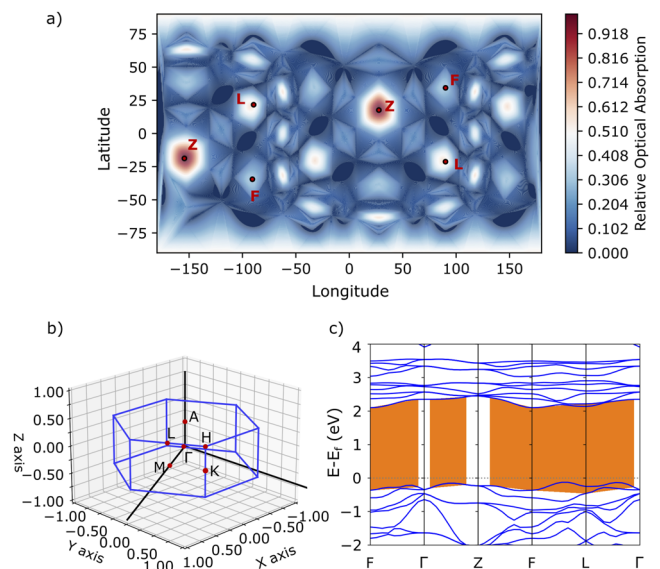
FIG. 4. (a) Spherical heat map of the direction-dependent optical absorption shown as a cylindrical projection along with the position and labels of the high symmetry points, (b) Brillouin zone, and (c) band structure plot for GaP. The shaded regions indicate momentum states, where vertical transitions are possible, when the photon energy is equal to E_g(GaP) + 1.5 eV.

that Pt deposits preferentially on rutile {110} facets, consistent with the band structure prediction. Instead, Günnemann et al.[28] showed (001) to be one of the rutile surfaces with the largest photonic efficiency and to be the most reactive surface for methanol
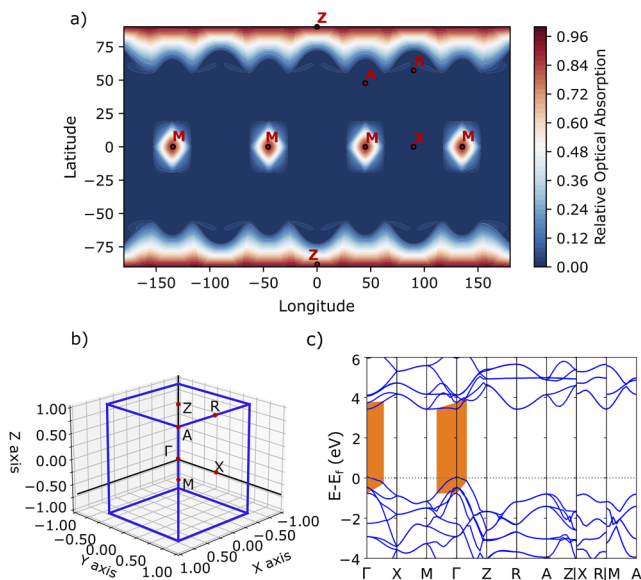
oxidation. This is in agreement with our prediction and also with the results of Ahmed et al.[29] reporting the (001) surface to show a higher photocatalytic activity than both the (110) and (100) surfaces for both methanol oxidation and terephthalic acid hydroxylation. Also, Lowekamp et al.[6] reported that {001} facets show a higher reactivity for Ag$^+$ reduction compared to the {110} and the {100} facets, even though the {101} facets are the most active. The larger photocatalytic activity of {101} surfaces was reported also by Giocondi and Rohrer,[7] Ohno et al.,[8] and Luttrell et al.[30] for decomposition of methyl orange or by Günnemann et al.[28] for terephthalic acid hydroxylation. On the other hand, Quah et al.[31] reported that there is no special photocatalytic activity of this latter facet compared to other rutile surfaces, together with our heat map that does not suggest the creation of carriers with momentum along this direction. Despite our data not being able to fully rationalize the controversial experimental results, they suggest that intrinsic direction-dependent surface properties due to both the anisotropy of the band structure and the TDM values could play a role.

A similar situation is observed also for Fe$_2$O$_3$. While the band structure in Fig. 6(c) shows fairly non-dispersive bands and, hence, possible transitions with momenta along different directions in space, the heat map of the direction-dependent optical absorption in Fig. 6(a) indicates that the (111) facet (transitions from Γ to Z) should be much more active than other surfaces. This prediction can also be rationalized by the larger TDM for a transition from the top of the VB to the bottom of the CB at the Z point (68.3 D^2), compared to the other high symmetry k-points, such as L (43.3 D^2) or F (10.3 D^2).

Finally, one has to consider that conventional band structures along a high-symmetry path do not show the band dispersion along

FIG. 5. (a) Spherical heat map of the direction-dependent optical absorption shown as cylindrical projection along with the position and labels of the high symmetry points, (b) Brillouin zone, and (c) band structure plot for TiO$_2$ rutile. The shaded regions indicate momentum states, where vertical transitions are possible, when the photon energy is equal to E_g(TiO$_2$-rutile) + 0.8 eV.

FIG. 6. (a) Spherical heat map of the direction-dependent optical absorption shown as cylindrical projection along with the position and labels of the high symmetry points, (b) Brillouin zone, and (c) band structure plot for Fe$_2$O$_3$. The shaded regions indicate momentum states, where vertical transitions are possible, when the photon energy is equal to E_g(Fe$_2$O$_3$) + 0.5 eV.
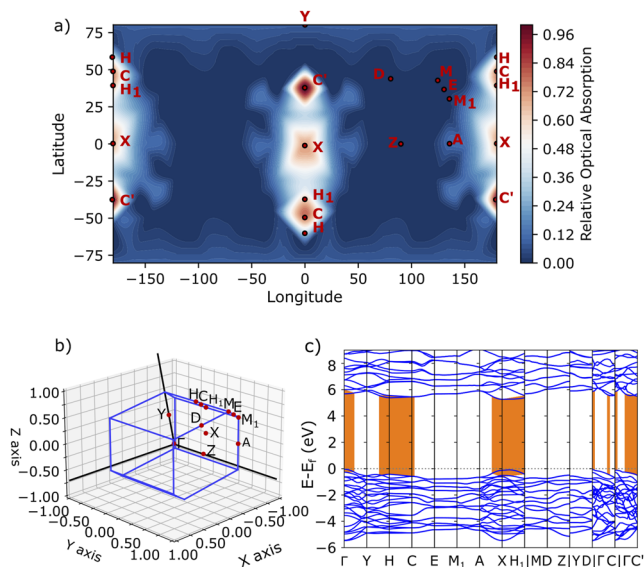
FIG. 7. (a) Spherical heat map of the direction-dependent optical absorption shown as cylindrical projection along with the position and labels of the high symmetry points, (b) Brillouin zone, and (c) band structure plot for ZrO_2. The shaded regions indicate momentum states, where vertical transitions are possible, when the photon energy is equal to $E_g(ZrO_2) + 0.8$ eV.

all directions. For example, the heat map for ZrO_2 in Fig. 7(a) suggests that the strongest absorption should occur at a point we indicated as C′ ([$\bar{1}0\bar{1}$] direction). The segment from Γ to C′ [see Fig. 7(c)] is indeed quite non-dispersive and definitely flatter than the segment from Γ to C ([$\bar{1}01$] direction), which is the one with the second strongest optical absorption in Fig. 7(a), but which is not reported in conventional band structure plots for ZrO_2.

These results not only show that our approach intrinsically takes into account the probability of a transition to happen via the calculation of the TDM, which was not considered in the original approach of Ref. 10 but also highlight that using only the dispersion of the conventional band structure to make predictions may not result in a complete description of the direction-dependent absorption properties. Figure 8 reports the heat maps for the selected photocatalysts computed for transitions in the energy range going from the bandgap of each material up to the minimum energy necessary to observe vertical transitions. These heat maps can be used to predict the anisotropic reactivity of different photocatalysts. For example, the (100) surface is predicted to be the most reactive surface for $SrTiO_3$, Cu_2O, HfO_2, SnO_2, and hexagonal SiC or together with the (001) surface for ZnO, and the hexagonal CdSe and CdS structures. Strong reactivity of the {001} facets is predicted for materials, such as WO_3, anatase, $CH_3NH_3PbI_3$, and Bi_2S_3. Finally, the (111) surface should be the most reactive not only for materials with the zinc-blend structure, as discussed above, but also for Si, Bi_2Se_3, Fe_2O_3, and $CsPbI_3$, while for the cubic SiC phase, a larger reactivity is expected for the {001} facets.

We stress here that our heat maps suggest which surfaces are perpendicular to directions with the largest number of

photo-generated carriers, but nothing ensures that these surfaces will necessarily be the most reactive in actual experiments. Phonon scattering can, for example, result in a change of the carrier momentum, implying that carrier mobility and mean free path need to be large for the carrier to reach a surface perpendicular to the initial direction.[10]

Furthermore, our approach does not take into account surface band bending and, hence, neither the band-edge position at different surfaces nor the possibility of surface or surface defect states to act as trapping or recombination centers.[10] Once at the surface, photo-generated carriers have to be efficiently transferred to acceptor/donor molecules, which may be preferentially absorbed on a surface different from the one with the largest number of carriers.[10,32] The stability and structural properties of the surface are also important; in some cases, the reactivity of a surface can be related to the type and number of exposed undercoordinated surface sites[33] or the most reactive surface may not be the most stable one.[34–37] For example, the larger photocatalytic activity of anatase nanoparticles with respect to rutile powders has sometimes been explained by the more active anatase (101) and (100) surfaces to be among the thermodynamically most stable surfaces.[29]

The mechanism of the studied redox process is also important. The above-mentioned contradictory results for rutile's reactivity were partially explained by some authors investigating oxidation and others reduction reactions. In addition, depending on experimental conditions, a reaction can happen following different mechanisms: for example, methanol is directly oxidized by photo-generated holes for the high methanol concentration, while for larger water content, the oxidation is mediated by hydroxyl radicals, thus resulting in a different reactivity of rutile surfaces for the same reaction but under different experimental conditions.[28]

Finally, the activity of a photocatalyst is strongly dependent on its physicochemical properties, such as the particle shape and size.[32] Giocondi et al.[10] suggested that different conclusions of various experimental works on rutile can also be rationalized by having been performed using either extended planar samples or single crystal particles. The reactivity of these two types of samples is hard to compare. A planar sample may exhibit a reduced reactivity compared to a surface with the same orientation on a microcrystal bounded by several different facets, because the planar specimen only contains a subset of the particle's surface sites and may, therefore, lack highly active sites for a given redox reaction.

Despite these limitations, our spherical heat maps contain information about a fundamental material property—the optical absorption and, hence, the ability to photo-generate carriers along a given direction—and can, thus, be used as a guide in material engineering to enhance the photocatalytic performance of a catalyst. Indeed, this intrinsic material property can be seen reflected in experimental results, even though to different extents, as the discussion related to $SrTiO_3$ and rutile-TiO_2 clearly shows. Our results, especially when combined with available experimental data, could, therefore, be a way to decide which surface orientations to explore when optimizing the photocatalytic activity of the materials we studied. However, due to the many additional factors affecting measurements, we cannot conclusively say to what extent our prediction will be in agreement with the experimental findings for each material.
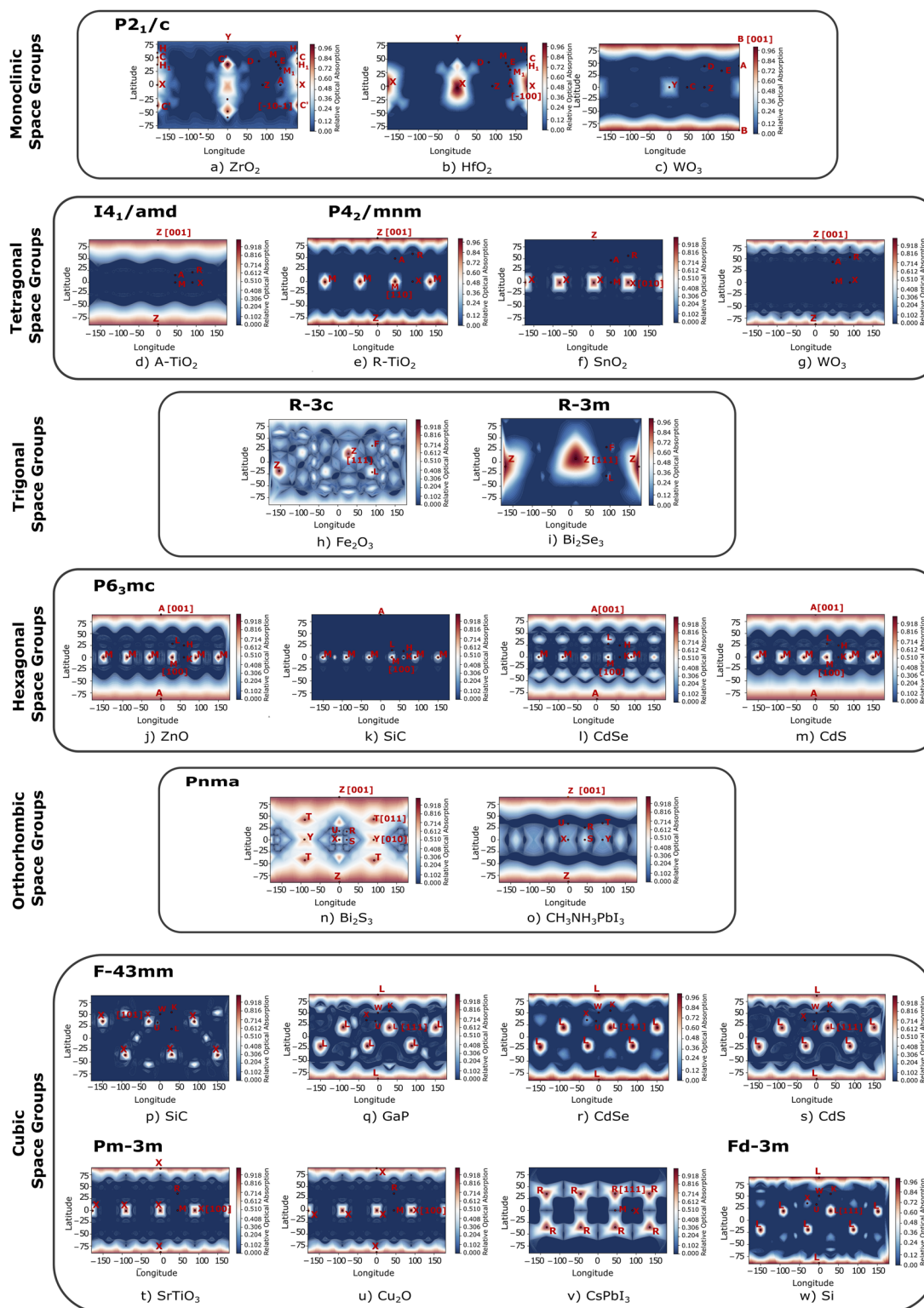
FIG. 8. Heat maps of the direction-dependent optical absorption for the selected photocatalysts. Transitions in the energy range from the bandgap (E_g) of each material up to $E_g + \Delta E$ eV (see Sec. II and Table S1 in the supplementary material) are taken into account.

IV. CONCLUSIONS

In the present work, the direction-dependent optical properties of different photocatalysts were investigated via hybrid DFT calculations to elucidate their anisotropic reactivity. The probability of a crystal to photo-generate carriers with momentum along a certain direction in space upon irradiation with light of a specific energy was mapped on the surface of a unit sphere centered on the origin of the reciprocal lattice to obtain 3D heat maps. For each point of the map, the contribution of all possible excited transitions weighted by their probability (transition-dipole matrix) was taken into account.

The results indicate that, in the majority of the cases, the pattern of the heat map, and hence the anisotropy of the photo-generated carriers, can be directly explained using the anisotropy of the band dispersion observed in conventional 2D band structure plots: the flatter the bands along one direction, the larger the number of photo-generated carriers with momentum in that direction, as suggested by Giocondi et al.[10] However, the results also suggest that 2D band structure plots are not always sufficient to understand the direction-dependence of the optical properties, but that weighing by a transition's probability according to the transition-dipole matrix can be crucial to obtain a complete picture.

Despite the possibility that the surface associated with the largest number of photo-generated carriers will not appear as most reactive in experiments, our approach captures a fundamental material property and can, thus, be invoked to predict the anisotropic reactivity of crystals to guide the design and development of highly efficient photocatalysts.

SUPPLEMENTARY MATERIAL

See the supplementary material for computational parameters (magnetism, pseudopotentials, k-meshes, and fraction of exact exchange) as well as primitive cells, computed structural and electronic properties, band structures, and Brillouin zones for all materials.

ACKNOWLEDGMENTS

AUTHOR DECLARATIONS

Conflict of Interest

The authors have no conflicts to disclose.

DATA AVAILABILITY

The data that support the findings of this study are openly available in Materials Cloud at https://doi.org/10.24435/materialscloud:2h-ca.

REFERENCES

[1] A. Fujishima and K. Honda, Nature 238, 37 (1972).
[2] S. Xie, Q. Zhang, G. Liu, and Y. Wang, Chem. Commun. 52, 35 (2016).
[3] X. Li, J. Yu, and M. Jaroniec, Chem. Soc. Rev. 45, 2603 (2016).
[4] S. Y. Tee, K. Y. Win, W. S. Teo, L.-D. Koh, S. Liu, C. P. Teng, and M.-Y. Han, Adv. Sci. 4, 1600337 (2017).
[5] S. San Martín, M. J. Rivero, and I. Ortiz, Catalysts 10, 901 (2020).
[6] J. B. Lowekamp, G. S. Rohrer, P. A. Morris Hotsenpiller, J. D. Bolt, and W. E. Farneth, J. Phys. Chem. B 102, 7323 (1998).
[7] J. L. Giocondi and G. S. Rohrer, J. Phys. Chem. B 105, 8275 (2001).
[8] T. Ohno, K. Sarukawa, and M. Matsumura, New J. Chem. 26, 1167 (2002).
[9] T. Taguchi, Y. Saito, K. Sarukawa, T. Ohno, and M. Matsumura, New J. Chem. 27, 1304 (2003).
[10] J. L. Giocondi, P. A. Salvador, and G. S. Rohrer, Top. Catal. 44, 529 (2007).
[11] F. Corà, M. Alfredsson, G. Mallia, D. S. Middlemiss, W. C. Mackrodt, R. Dovesi, and R. Orlando, "The performance of hybrid density functionals in solid state chemistry," in Principles and Applications of Density Functional Theory in Inorganic Chemistry II (Springer, Berlin, Heidelberg, 2004), pp. 171–232.
[12] E. N. Brothers, A. F. Izmaylov, J. O. Normand, V. Barone, and G. E. Scuseria, J. Chem. Phys. 129, 011102 (2008).
[13] T. M. Henderson, J. Paier, and G. E. Scuseria, Phys. Status Solidi B 248, 767 (2011).
[14] M. Gajdoš, K. Hummer, G. Kresse, J. Furthmüller, and F. Bechstedt, Phys. Rev. B 73, 045112 (2006).
[15] J. Wang, H. Chen, S. H. Wei, and W. J. Yin, Adv. Mater. 31, 1806593 (2019).
[16] M. Nishiwaki and H. Fujiwara, Comput. Mater. Sci. 172, 109315 (2020).
[17] M. Dresselhaus et al., Lecture Notes, Massachusetts Institute of Technology, Cambridge, MA, 2001, Vol. 17, p. 15.
[18] G. Kresse and J. Hafner, Phys. Rev. B 47, 558 (1993).
[19] G. Kresse and J. Hafner, Phys. Rev. B 49, 14251 (1994).
[20] G. Kresse and J. Furthmüller, Comput. Mater. Sci. 6, 15 (1996).
[21] G. Kresse and J. Furthmüller, Phys. Rev. B 54, 11169 (1996).
[22] J. Heyd, G. E. Scuseria, and M. Ernzerhof, J. Chem. Phys. 118, 8207 (2003).
[23] J. Heyd and G. E. Scuseria, J. Chem. Phys. 121, 1187 (2004).
[24] P. E. Blöchl, Phys. Rev. B 50, 17953 (1994).
[25] G. Kresse and D. Joubert, Phys. Rev. B 59, 1758 (1999).
[26] S. P. Ong, W. D. Richards, A. Jain, G. Hautier, M. Kocher, S. Cholia, D. Gunter, V. L. Chevrier, K. A. Persson, and G. Ceder, Comput. Mater. Sci. 68, 314 (2013).
[27] V. Wang, N. Xu, J.-C. Liu, G. Tang, and W.-T. Geng, Comput. Phys. Commun. 267, 108033 (2021).
[28] C. Günnemann, C. Haisch, M. Fleisch, J. Schneider, A. V. Emeline, and D. W. Bahnemann, ACS Catal. 9, 1001 (2019).
[29] A. Y. Ahmed, T. A. Kandiel, T. Oekermann, and D. Bahnemann, J. Phys. Chem. Lett. 2, 2461 (2011).
[30] T. Luttrell, S. Halpegamage, J. Tao, A. Kramer, E. Sutter, and M. Batzill, Sci. Rep. 4, 4043 (2014).
[31] E. L. Quah, J. N. Wilson, and H. Idriss, Langmuir 26, 6411 (2010).
[32] H. L. Tan, X. Wen, R. Amal, and Y. H. Ng, J. Phys. Chem. Lett. 7, 1400 (2016).
[33] Y. Su, H. Li, H. Ma, J. Robertson, and A. Nathan, ACS Appl. Mater. Interfaces 9, 8100 (2017).
[34] S. H. Chang, N. Danilovic, K.-C. Chang, R. Subbaraman, A. P. Paulikas, D. D. Fong, M. J. Highland, P. M. Baldo, V. R. Stamenkovic, J. W. Freeland, J. A. Eastman, and N. M. Markovic, Nat. Commun. 5, 4191 (2014).
[35] S. H. Chang, J. G. Connell, N. Danilovic, R. Subbaraman, K.-C. Chang, V. R. Stamenkovic, and N. M. Markovic, Faraday Discuss. 176, 125 (2014).
[36] N. Danilovic, R. Subbaraman, K.-C. Chang, S. H. Chang, Y. J. Kang, J. Snyder, A. P. Paulikas, D. Strmcnik, Y.-T. Kim, D. Myers, V. R. Stamenkovic, and N. M. Markovic, J. Phys. Chem. Lett. 5, 2474 (2014).
[37] C. Roy, R. R. Rao, K. A. Stoerzinger, J. Hwang, J. Rossmeisl, I. Chorkendorff, Y. Shao-Horn, and I. E. L. Stephens, ACS Energy Lett. 3, 2045 (2018).